Numerical simulation of vortices with axial velocity deficits

Saad Ragab and Madhu Sreedhar

Citation: Physics of Fluids (1994-present) **7**, 549 (1995); doi: 10.1063/1.868582
View online: http://dx.doi.org/10.1063/1.868582
View Table of Contents: http://scitation.aip.org/content/aip/journal/pof2/7/3?ver=pdfcov
Published by the AIP Publishing

Numerical simulation of vortices with axial velocity deficits

Saad Ragab
Department of Engineering Science and Mechanics, Virginia Polytechnic Institute and State University, Blacksburg, Virginia 24061

Madhu Sreedhar
Institute of Hydraulic Research, University of Iowa, Iowa City, Iowa 52242

(Received 31 May 1994; accepted 31 October 1994)

Axial velocity deficit is a source of instability in vortices that may otherwise be stable. Temporal large-eddy simulation is performed to study the response of vortices with axial velocity deficits to random and controlled disturbances at high Reynolds numbers. The q vortex [Batchelor, J. Fluid Mech. **20**, 321 (1964)] is used as a model of such vortices. When the vortex is linearly unstable, the disturbances grow and result in the appearance of large-scale helical sheets of vorticity. Later, these large-scale helical structures break up into small-scale filaments. Associated with the formation of the large-scale structures is a redistribution of both angular and axial momentum between the core and the surroundings. The redistribution weakens the axial velocity deficit in the core while strengthens the rigid-body-like rotation of the core. The emerging mean velocity profiles drive the vortex core to a stable configuration. The vortex eventually returns to a laminar state, with an insignificant decay in the tangential velocity, but with a much weakened axial velocity deficit. A direct numerical simulation obtained at a lower Reynolds number confirms the above conclusions. © *1995 American Institute of Physics.*

I. INTRODUCTION

Wakes shed by lifting bodies roll up and form strong streamwise vortices. The trailing vortices shed by a large aircraft pose a serious threat to a following smaller aircraft. Such powerful vortices are also shed from a submarine during a rapid maneuver, and they tend to persist in the far wake. The turbulence in the wake shed by the lifting body gets engulfed into the vortex core during its formation. The decay of these fluctuating quantities, as well as the possibility of generating new large-scale structures, depend on the stability characteristics of the resulting mean flow field.

Rayleigh[1] developed a formal theory for the stability of swirling flows. His work was on the effects of axisymmetric disturbances on revolving fluids. Rayleigh's circulation criterion states that a necessary and sufficient condition for the stability of swirling flow fields to axisymmetric disturbances is that the square of the circulation does not decrease anywhere in the flow field. The Lamb–Oseen vortex is an example of a stable vortex. An example of a centrifugally unstable vortex is the Taylor vortex. Both of these vortices are exact solutions to the unsteady incompressible Navier–Stokes equations (see Panton[2] for details). Using large-eddy simulation (LES), Sreedhar and Ragab[3] have studied the effect of random disturbances on the stability of these vortices. They found that the disturbances superimposed on the Taylor vortex were amplified and the vortex went through a transition process, which resulted in the decay of the mean flow. On the other hand, the disturbances superimposed on the Lamb–Oseen vortex were damped, and the mean flow showed no decay. Their simulations were for vortices with no axial velocity.

A destabilizing mechanism of vortices with monotonically increasing circulation is a jet-like or wake-like axial velocity deficit. Batchelor and Gill[4] derived a necessary condition for the instability of nonswirling axisymmetric shear flows. They found that a top hat or a fully developed jet satisfies that necessary condition. Therefore, the presence of a sufficiently strong axial velocity deficit may render a swirling flow unstable, even if the circulation is monotonically increasing with the radius. Uberoi *et al.*[5] and Narain and Uberoi[6] showed that a difference in axial velocity between the core and the surroundings destabilizes swirling flows that are otherwise stable. This destabilizing role of the axial velocity field in trailing vortices has been experimentally observed by Singh and Uberoi.[7]

Batchelor[8] derived an asymptotic solution for trailing vortices in the far wake of a lifting surface. The q vortex[9] is a simplified version of the Batchelor vortex. Most of the investigative works on the stability of vortices in the past two decades used the q vortex as a model. The circulation profile of the q vortex is identical to the Lamb–Oseen vortex, which is centrifugally stable. But the vortex possesses an axial velocity profile, which makes the vortex vulnerable to shear flow instabilities. The q vortex is characterized by a swirl parameter q, which is proportional to the ratio of the magnitude of the maximum swirl velocity to that of the maximum axial velocity deficit or excess. Lessen *et al.*[9] and Lessen and Paillet[10] presented inviscid and viscous calculations of the stability characteristics for a q vortex. They found that increasing the swirl parameter q above 1.5 stabilized all the modes, regardless of their orientations. Duck and Foster[11] found a continuous spectrum of unstable modes for the q vortex subjected to inviscid disturbances. The spectrum contained an infinite number of higher modes for each combination of the axial wave number, azimuthal wave number, and the swirl parameter q. This multiplicity of modes is a very interesting feature of the q vortex, which makes the problem very unique. Khorrami[12] used Chebyshev spectral collocation technique to obtain highly accurate linear stabil-

ity results for a q vortex, including viscous effects. He showed that the higher inviscid modes persist for much lower Reynolds numbers. He also discovered two unstable viscous modes. The growth rates of these modes were found to increase with Reynolds number initially and then decrease. These viscous modes were found to be less dangerous than the inviscid modes, since their growth rates are an order of magnitude less than the inviscid modes. Duck and Khorrami[13] extended Khorrami's work, focusing on the viscous modes. Using a spectral collocation and matrix eigenvalue method, Mayer and Powell[14] mapped the entire unstable region in the swirl-/axial-wave number space for various azimuthal wave numbers. Other than these numerical computations, the q vortex has attracted many investigators, including Stewartson[15] and Leibovitch and Stewartson,[16] who used asymptotic methods to study the stability characteristics.

From the above review, we see that the linear stability characteristics of the q vortex as a model of aircraft trailing vortices are well documented. However, very little is known about the relevance of such instability waves to the production of turbulence in vortices or the fate of these waves in the nonlinear range. The turbulent structure of the vortex is decided by the relative strength of the swirl component to the axial velocity deficit. If the axial velocity deficit is sufficiently strong, new large-scale structures may develop, as a result of the instability of such a vortex. The large-scale structures extract energy from the mean flow, and the vortex may undergo a transition period, resulting in a turbulent flow field. An interesting situation results if the axial velocity deficit is weakened by that energy transfer. The combination of a weaker axial velocity deficit and a swirling flow may become linearly stable, and the production of new large-scale structures ceases. As a result of this, there is no mechanism to feed energy into the turbulence, which will eventually lead the mean flow to relaminarize.

Objective: The main objectives of this work can be summarized as follows.

To study the response of vortices with axial velocity deficits to controlled and random initial disturbances using LES.

To identify the large-scale structures that are formed due to nonlinear interaction of unstable modes and their effect on the structure of the vortex.

II. EQUATIONS AND METHOD OF SOLUTION

The premise of LES is that only small scales, which tend to be isotropic and hence more universal in nature, need to be modeled. Furthermore, the small scales carry a small portion of the total turbulent energy, and thus one anticipates that the subgrid-scale (SGS) models are less complicated than the turbulence models required for the Reynolds-averaged equations. The majority of LES results obtained to date used an eddy-viscosity model. The eddy-viscosity coefficient is usually determined from the Smagorinsky model.[17] Another eddy-viscosity SGS model gaining popularity is the dynamic model devised by Germano *et al.*[18] In this model, the Smagorinsky constant is computed dynamically as the calculation progresses rather than input *a priori*. This results in a turbulence model coefficient that can vary temporally and spatially, depending on the flow field.

The Navier–Stokes equations are Favre filtered. Let an overtilde denote a Favre-filtered quantity and an overbar denote the space filtering operation. Following Erlebacher *et al.*,[19] we introduce the Favre-filtered field,

$$\tilde{f}=\frac{\overline{\rho f}}{\bar{\rho}}, \tag{1}$$

and decompose the total flow field into a resolvable field $\tilde{f}$ and a subgrid-scale field f',

$$f=\tilde{f}+f'. \tag{2}$$

Filtering the mass and momentum equations, we obtain

$$\frac{\partial\bar{\rho}}{\partial t}+\frac{\partial(\bar{\rho}\tilde{u}_j)}{\partial x_j}=0, \tag{3}$$

$$\frac{\partial\bar{\rho}\tilde{u}_i}{\partial t}+\frac{\partial}{\partial x_j}(\bar{\rho}\tilde{u}_i\tilde{u}_j+\bar{p}\,\delta_{ij}+R_{ij}-\bar{\tau}_{ji})=0, \tag{4}$$

where

$$R_{ij}=\bar{\rho}(\widetilde{u_iu_j}-\tilde{u}_i\tilde{u}_j) \tag{5}$$

is the subgrid-stress tensor and $\bar{\tau}_{ij}$ is the viscous stress tensor. The filtered pressure is given by

$$\bar{p}=\bar{\rho}R\tilde{T}, \tag{6}$$

where $\tilde{T}$ is the resolvable temperature field and R is the gas constant.

Filtering the total energy equation, we obtain

$$\frac{\partial(\bar{\rho}\tilde{E}+k)}{\partial t}+\frac{\partial}{\partial x_j}[(\bar{\rho}\tilde{E}+\bar{p})\tilde{u}_j+K_j+Q_j-\overline{u_i\tau_{ji}}+\overline{q_j}]=0, \tag{7}$$

where

$$\tilde{E}=\tilde{e}+\tfrac{1}{2}\tilde{u}_i\tilde{u}_i, \tag{8}$$

$$Q_j=C_p\bar{\rho}(\widetilde{Tu}_j-\tilde{T}\tilde{u}_j), \tag{9}$$

$$k=\tfrac{1}{2}(R_{ii}), \tag{10}$$

and

$$K_j=\tfrac{1}{2}\bar{\rho}(\widetilde{u_iu_iu_j}-\tilde{u}_i\tilde{u}_i\tilde{u}_j). \tag{11}$$

The Smagorinsky[17] formula is used to model the subgrid stress tensor. The model constants are computed using the dynamic procedure of Germano *et al.*[18] For a complete discussion on the model including derivation and implementation, see Sreedhar[20] and Sreedhar and Ragab.[3]

The numerical scheme used for LES in this investigation is a modified MacCormack scheme developed by Gottlieb and Turkel.[21] This scheme is fourth order in space for the convective terms and second order for the diffusion terms and time. More details of the method can be found in Gottlieb and Turkel[21] and Ragab *et al.*[22] Implementation of this scheme for vortex simulations and code validation using linear stability results are given in Sreedhar[20] and Sreedhar and Ragab.[3] Direct numerical simulation presented here is obtained, using a combination of spectral (in the streamwise

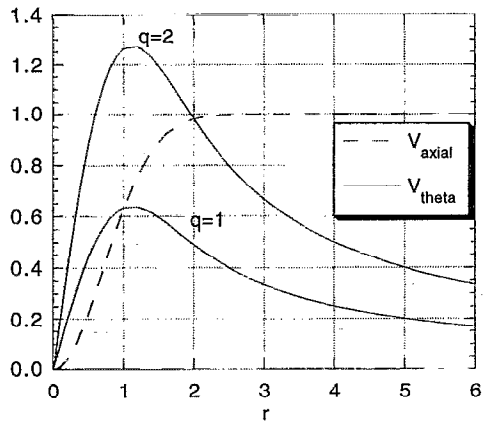

FIG. 1. Mean velocity profiles for the q vortex. The tangential velocity is plotted for two different values of q.

direction) and sixth-order compact finite-difference scheme[23] in the two transverse directions. The time integration is by a low-storage third-order Runge–Kutta scheme.

III. RESULTS AND DISCUSSION

Temporal simulation is performed, so that adequate grid resolution can be obtained. The simulations are for a low subsonic Mach number of 0.2 based on the free-stream values, which should bring the calculations very near the incompressible limit.

A. Initial conditions and computational domain

The tangential velocity of the q vortex is given by

$$U_\theta=\frac{q}{r}(1-e^{-r^2}), \tag{12}$$

and the axial component of the velocity is given by

$$U_x=1-e^{-r^2}. \tag{13}$$

As seen from the above equations, the q vortex has a tangential velocity profile identical to the Lamb–Oseen vortex, which is stable to axisymmetric inviscid disturbances. The axial velocity profile has a deficit of unity that renders the q vortex susceptible to linear disturbances, depending on the value of q. The tangential and axial velocity profiles for the q vortex are shown in Fig. 1. The stability characteristics of the q vortex are unaffected by the addition or subtraction of a constant U_∞ to the axial velocity profile or by the inversion of the wake-like profile to a jet-like profile.

The reference length δ_0 is related to the initial core radius r_c by $\delta_0=0.892r_c$. The reference velocity V_0 is the initial axial velocity deficit. The Reynolds number based on reference parameters is 50 000.

A total of $N_x=49$ points is used in the streamwise direction, while $N_y=N_z=97$ points are used in the cross-plane $(Y-Z)$. The grid is stretched in the cross-plane so that the vortex core is described with 21 grid points in the diameter. Periodic boundary conditions are imposed in the streamwise direction (X) and symmetry boundary conditions are applied in the other two directions $(Y-Z)$ in the cross-plane (see

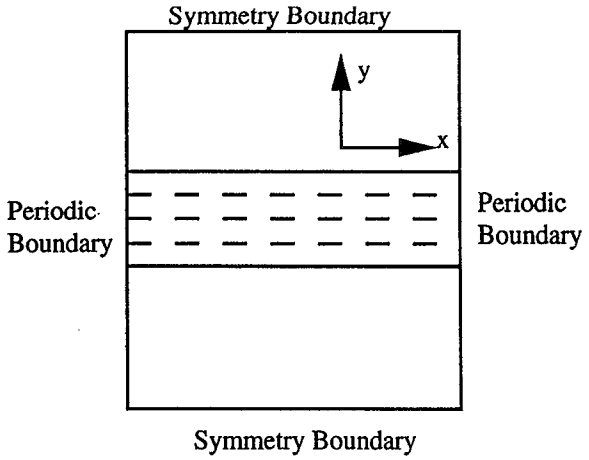

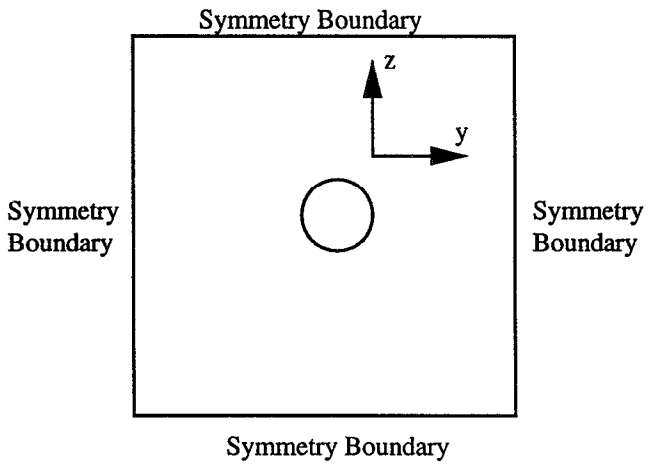

FIG. 2. Computational domain and boundary conditions. The vortex core is exaggerated relative to the outer boundary.

Fig. 2). The application of symmetry boundary conditions in the cross-plane has been shown to be adequate for vortex simulations by Sreedhar[20] and Sreedhar and Ragab,[3] provided the initial mean tangential velocity is small in the far field.

The computational domain extends from $-30\delta_0$ to $+30\delta_0$ in each direction of the cross- $(Y-Z)$ plane, which is sufficient for the initial mean tangential velocity to decay by an order of magnitude compared to the core velocity. Moreover, the induced velocity by the nearest image vortices in the region of observed turbulent activity is less than 0.3% of the maximum tangential velocity. The length of the computational domain in the streamwise direction (X) is $2\pi/\alpha$, where α is the streamwise wave number at maximum amplification of the lowest helical mode of linear stability. Linear stability analysis also shows that higher-order unstable modes exist at higher azimuthal mode numbers, but with lesser axial wavelengths. Therefore, the chosen computational domain is large enough for these unstable higher-order modes to grow and interact with each other.

Two cases are studied.

Case A: The purpose of this run is to study the effect of

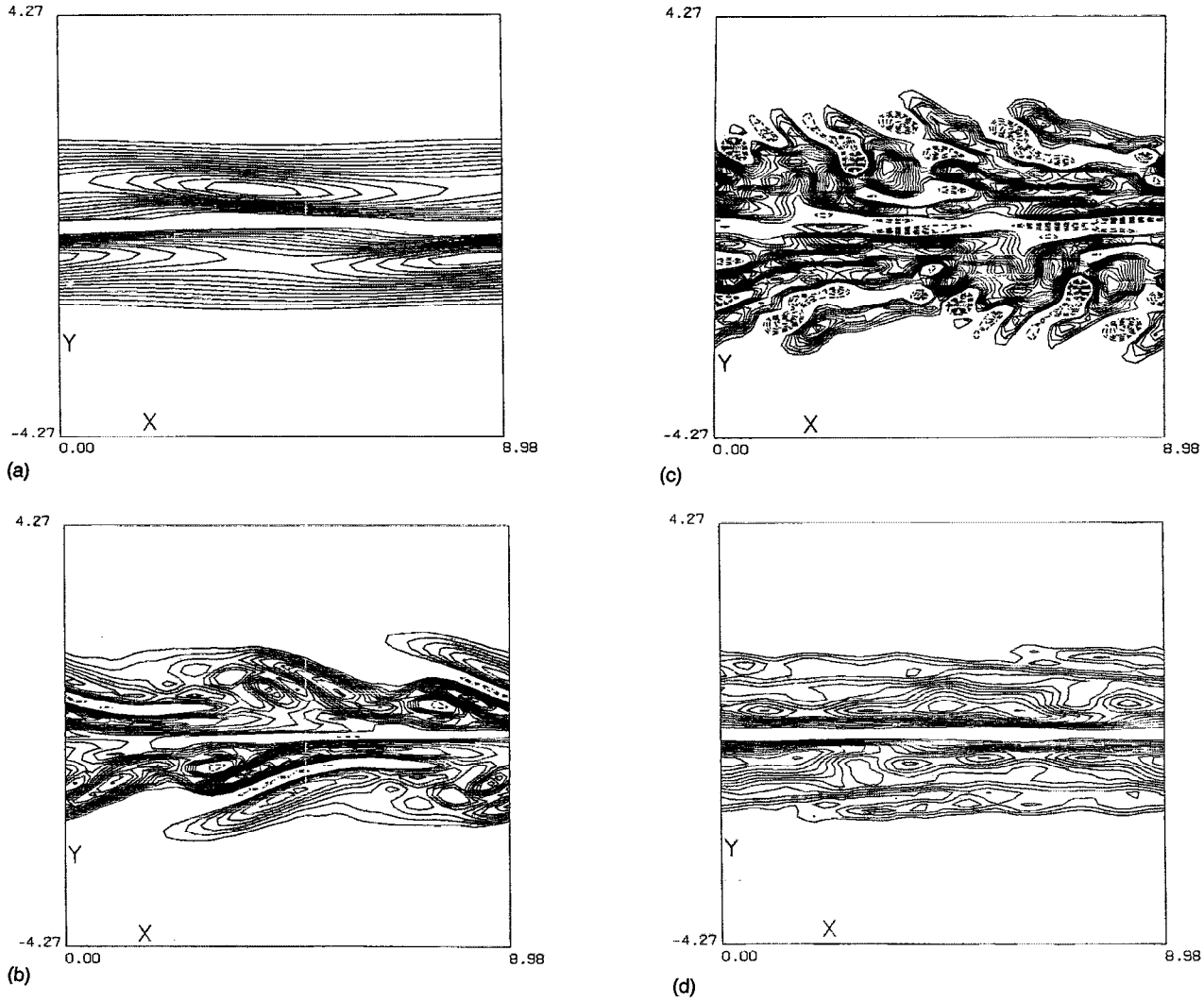

FIG. 3. Azimuthal vorticity contours in a meridional $(X-Y)$ plane for the q vortex. The mean flow is pertrubed with the (1,1) mode. (a) $Time=8$, $\omega_{max}=0.15$, and $\omega_{min}=-1.05$. (b) $Time=28$, $\omega_{max}=0.34$, and $\omega_{min}=-1.86$. (c) $Time=48$, $\omega_{max}=0.85$, and $\omega_{min}=-1.31$. (d) $Time=138$, $\omega_{max}=0.11$, and $\omega_{min}=-0.83$.

controlled disturbances on the development of large-scale structures and the subsequent fate of the vortex. The value of q is taken to be unity. At this level of q, the vortex is unstable to linear disturbances. An unstable linear stability wave, the helical (1,1) mode and its complex conjugate, is superposed on the mean flow. This mode corresponds to $\alpha=0.7$ and azimuthal wave number $m=1$. The maximum amplitude of the radial disturbance velocity is taken to be two percent of the mean axial velocity deficit.

In this case, the mean pressure is obtained by integrating the radial momentum equation,

$$\frac{\partial p}{\partial r}=\frac{\rho U_\theta^2}{r}. \tag{14}$$

Case B: The purpose of this run is to determine the response of a linearly stable q vortex to strong initial disturbances. In this case, the value of q is 2. At this level of q the vortex is stable to linear disturbances. Therefore, strong random disturbances are used to initialize the flow. The RMS value of the disturbance is taken to be ten percent of the mean axial velocity deficit. At this amplitude the disturbances are well above the linear range. The initial pressure field for case B is obtained by solving the equation

$$\nabla^2 p=-\frac{\partial u_i}{\partial x_j}\frac{\partial u_j}{\partial x_i}, \tag{15}$$

where u_i denotes the total velocity field and ∇^2 is the Laplacian operator.

B. Large-scale structures

Contours of azimuthal and streamwise vorticity are used to describe the evolution of large-scale structures. Negative values of vorticity are shown by solid lines and positive values by dashed lines.

Shown in Figs. 3(a)–3(d) are the azimuthal vorticity contours in a meridional plane $(X-Y)$ at different times. Initially, the contours are straight lines, except near the center of the core, as shown in Fig. 3(a), which shows the contours at $T=8$. Only negative vorticity is visible at this time. The high values of negative vorticity is due to the strong wake-like mean axial flow. This well-organized core distorts and branches out in the form of helical vortex sheets. These

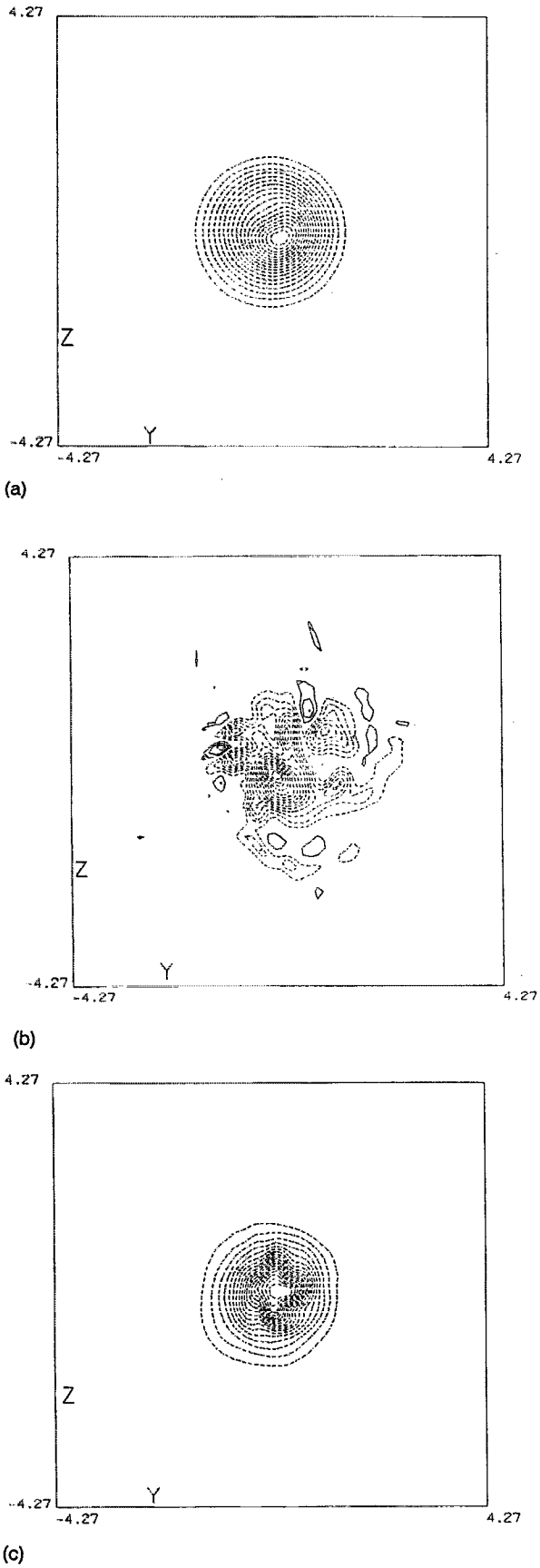

FIG. 4. Streamwise vorticity contours in a cross- $(Y-Z)$ plane for the q vortex. The mean flow is perturbed with the (1,1) mode. (a) $Time=8$, $\omega_{max}=2.19$, and $\omega_{min}=0.00$. (b) $Time=48$, $\omega_{max}=3.93$, and $\omega_{min}=-0.93$. (c) $Time=152$, $\omega_{max}=2.67$, and $\omega_{min}=-0.03$.

branches flaring out of the vortex core can be seen on the azimuthal vorticity contours at $T=28$, shown in Fig. 3(b). Later, these sheets, due to self-induction, break up into helical filaments that reside in the otherwise irrotational flow surrounding the core. This breakup of the vortex sheets is evident in Fig. 3(c), which shows the azimuthal vorticity contours at $T=48$. Regions of positive azimuthal vorticity are also seen embedded in the flow field surrounding the core. The presence of positive and negative vorticity regions embedded within each other is an indication of the generation of small-scale motions. These structures, which originated just outside the core, persist for a relatively long period of time, but eventually decay and the vortex returns to a laminar state. The azimuthal vorticity contours at $T=138$, as shown in Fig. 3(d), confirm this conclusion, since no small-scale motion is visible at this time. As will be shown later, this apparent return of the vortex to a laminar configuration is due to the cessation of the production of new large-scale structures due to the weakening of the instability mechanism, and to the dissipative nature of the vortex core that quenches the existing turbulence.

Streamwise vorticity contours in the cross-plane $(Y-Z)$ shown in Figs. 4(a)–4(c), also reveal a similar trend. At $T=8$, the vortex core shows no sign of small-scale motions, as is evident in Fig. 4(a). Since the mean vorticity is positive and the disturbances have not yet grown to any significant level, only positive vorticity (dashed lines) can be seen at this time. At $T=48$, we see a marked change in the contour pattern given in Fig. 4(b). Also seen in Fig. 4(b) are solid-line contours, indicating the presence of negative streamwise vorticity. As observed earlier from the sequence of azimuthal contours in the meridional plane $(X-Y)$, these new structures that are formed at this instant in time disappear as the simulation progresses in time. The contours at $T=152$, shown in Fig. 4(c), are similar to the ones at $T=8$ shown in Fig. 4(a).

For case B, where high-amplitude random disturbances are used to perturb a linearly stable q vortex, the structures are not well organized and they disappear very quickly. Therefore, they are not presented here.

A study of the evolution of large-scale structures in a q

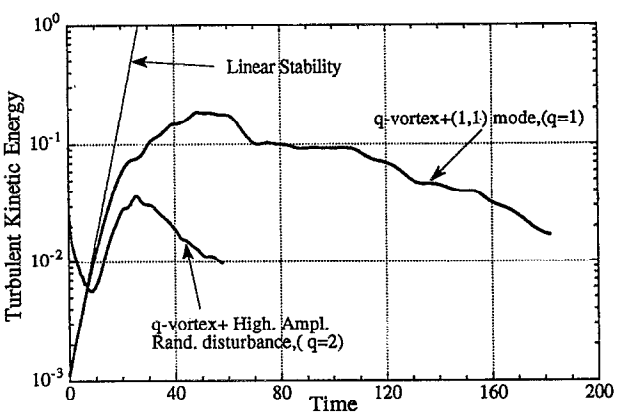

FIG. 5. Evolution of turbulent kinetic energy for the q vortex for different initial conditions.

vortex reveals the following behavior. The instability mechanism due to the strong axial velocity deficit results in the production of large structures in the form of helical sheets of vorticity. Later, these structures break up into concentrated helical filaments around the core. As will be shown later, the interaction of these large-scale structures has a profound redistribution effect on the mean axial and tangential velocities, which tends to weaken the instability mechanism. The weakening of the instability mechanism adversely affects the production process of new large-scale structures. Meanwhile, the small-scale motions are subjected to the stabilizing mechanism of the strong rigid-body-like flow field. Thus, the combined effect of a weakening instability mechanism and the stabilizing feature of the swirling flow field drives the vortex to a laminar configuration. The weakening of the instability mechanism will be revisited in Sec. III D, where the evolution of mean velocity is described. The relaminarizing tendency of the care of a trailing vortex has been observed experimentally by Bandhyopathay *et al.*[24] They state that "At quasi-periodic intervals, the core receives a patch of turbulent fluid from the fully turbulent outer annulus where it is subsequently relaminarized by the centrifugal motion." The laminar nature of the vortex core in the wake of a rectangular wing has also been observed in the experiments of Devenport *et al.*[25]

C. Turbulent kinetic energy

The growth and decay of the turbulent kinetic energy is studied in this section.

At any point in time, the Cartesian velocity components are first resolved into polar components at the Cartesian computational grid points. Then these components are averaged in the axial direction. Second, the three components are interpolated into a polar grid and averaged in the θ direction. This procedure provides mean velocity profiles that are functions of r only. Note that no time averaging is performed, and as a result the mean profiles thus defined change in time.

The total turbulent kinetic energy is obtained by integrating over the $Y-Z$ plane the quantity

$$E(y,z,t)=\tfrac{1}{2}\langle u'^2+v'^2+w'^2\rangle_x,$$

where $\langle\cdots\rangle_x$ indicates averaging in the axial direction. Here,

$$u'=\tilde{u}-\langle\tilde{u}\rangle,$$

where $\langle\tilde{u}\rangle$ is the mean velocity. Similar expressions are used for v' and w'.

Recall that in case A the initial perturbations consist of a linear stability wave while in case B high-amplitude random perturbations are used. In case A, the turbulent kinetic energy grows rapidly in the initial stages, as shown in Fig. 5. This strong growth in the early stages is primarily due to the amplification of the linear stability wave seeded in the initial conditions. As expected, the initial growth rate of energy agrees well with the linear stability theory. Once this wave is sufficiently amplified, it starts to interact nonlinearly with itself and with the mean flow resulting in the amplification of high-order modes. Later, the kinetic energy saturates and a period of very slow decay is observed. The saturation of the energy is found to occur between times $T=50$ and $T=80$. The distribution of turbulent kinetic energy E on the Y axis at different times is shown in Fig. 6. The kinetic energy distribution at $T=57$ shows very high values in the regions in and around the core. Later, as the core relaminarizes, the kinetic energy drops to its initial levels. Note that the kinetic energy levels at $T=8$ and $T=182$ are comparable.

Also shown in the Fig. 5 is the evolution of total turbulent kinetic energy for case B. In this case, the total turbulent kinetic energy initially decreases. This is due to the reorganization of the high-amplitude nonphysical initial conditions. Later, due to the growth of local instabilities the kinetic energy increases. This growth is attributed to the presence of local instabilities presumably of the centrifugal type. The nature of these local instabilities needs further investigation. But, before long, the kinetic energy saturates and it starts to

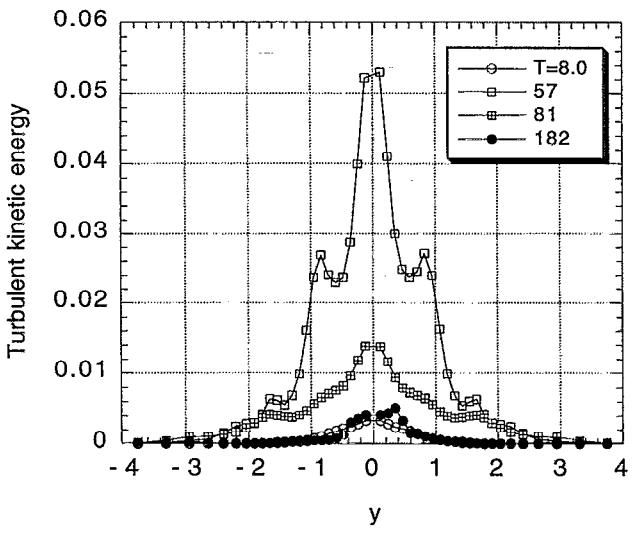

FIG. 6. Radial distribution of turbulent kinetic energy for the q vortex at different times. The mean flow is perturbed with the (1,1) mode.

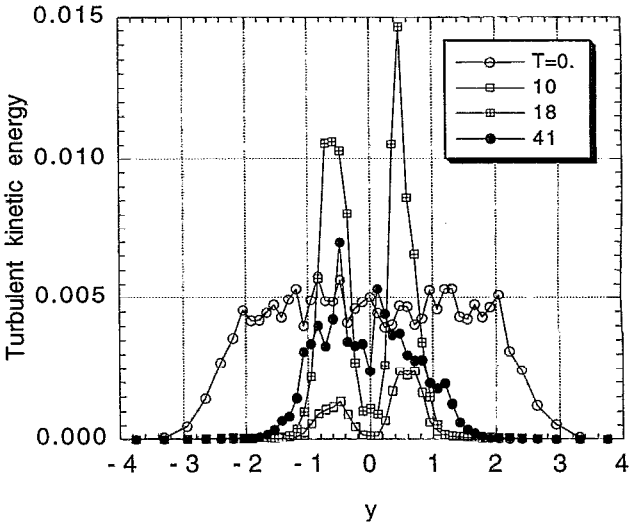

FIG. 7. Radial distribution of turbulent kinetic energy for the q vortex at different times. The flow is perturbed with high-amplitude random disturbances.

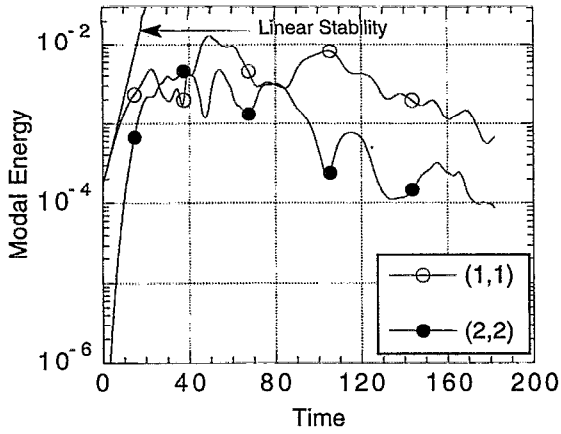

FIG. 8. Evolution of modal kinetic energy for the (1,1) mode and the (2,2) mode for the q vortex for case A, where the initial perturbation consists of the (1,1) mode. The curve predicted by the linear stability is also marked.

decay. The decay rate is more rapid in case B than in case A. This proves that the presence of local instabilities is not enough to sustain the production of large-scale motions.

The radial distribution of the kinetic energy at different times for case B is shown in Fig. 7. Note that the kinetic energy growth is the strongest outside the core. Also, the maximum level of kinetic energy in case B is much lower than that in case A, because of the stronger swirling velocity field present in case B. At higher swirl velocities, the axial velocity deficit could not produce large-scale structures, and the subsequent generation of small-scale motions is suppressed.

The growth of some of the helical modes are shown in Fig. 8 for case A. The modal energies of the (1,1) mode and the (2,2) mode, which corresponds to $\alpha=0.7$, $m=1$ and $\alpha=1.4$, $m=2$, respectively, are shown. The (1,1) mode that is initially seeded starts at a higher-energy level and grows according to the linear stability predictions in the early stages. The (2,2) mode also shows strong growth, and at one instant is more energetic than the (1,1) mode. This growth of

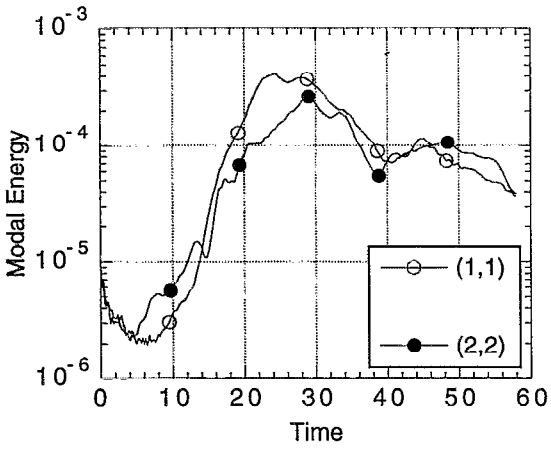

FIG. 9. Evolution of modal kinetic energy for the (1,1) mode and the (2,2) mode for the q vortex for case B, where the initial perturbation consists of high-amplitude random disturbances.

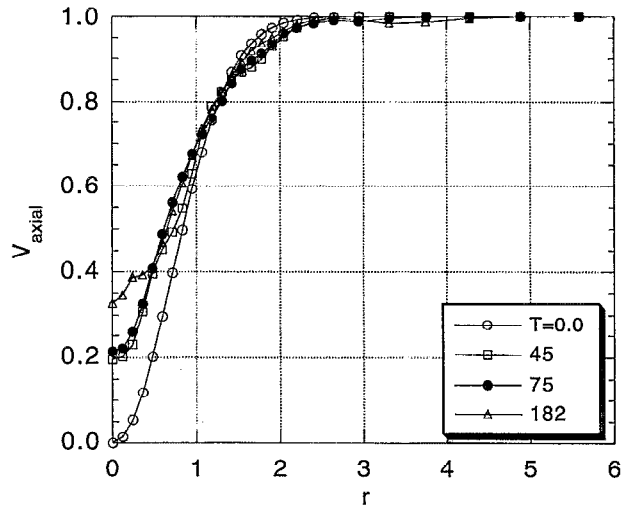

FIG. 10. Decay of the mean axial velocity profile for the q vortex for case A, where the initial perturbation consists of the (1,1) mode.

the (2,2) mode is attributed to nonlinear interactions, because this mode was not initially seeded. Later, these two modes show a saturation trend followed by a slow decay. The same two modes for case B, which was perturbed by random disturbances, are shown in Fig. 9. Both of these modes show an initial decay followed by periods of amplification, saturation, and decay. The levels of energy in these modes are much less than that in the corresponding modes for case A shown in Fig. 8. Other higher modes also displayed a similar trend.

D. Mean velocity and comparisons with experiments

From the previous two sections we have seen that the growth and decay of the turbulent kinetic energy is associated with the growth and decay of vortical structures. The influence of these events on the mean velocity profiles is discussed in this section. Figures 10 and 11 show the devel-

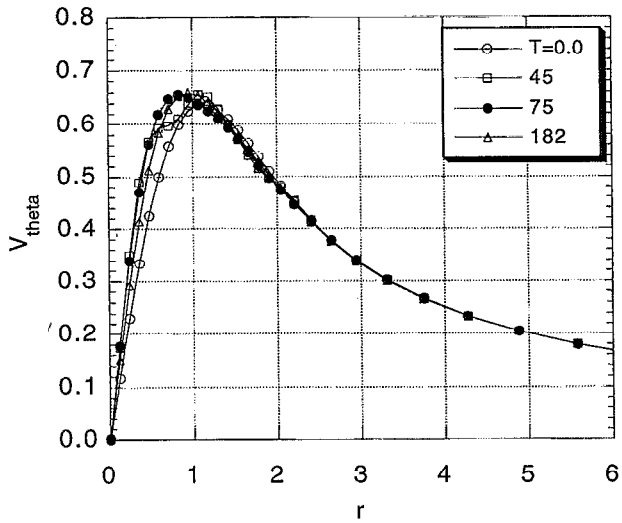

FIG. 11. Evolution of the mean tangential velocity profile for the q vortex for case A, where the initial perturbation consists of the (1,1) mode.

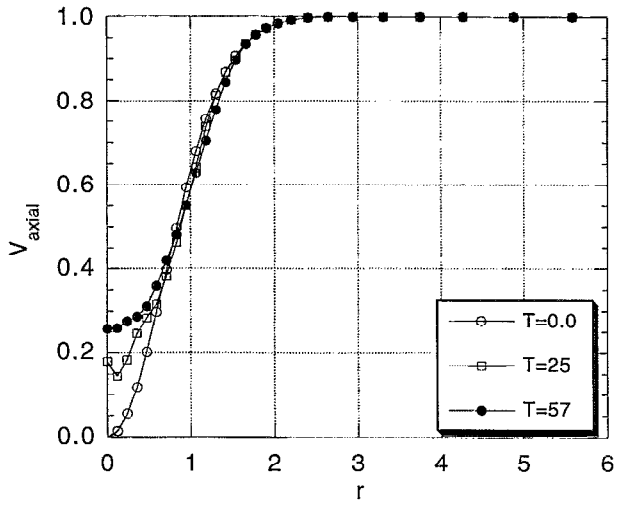

FIG. 12. Decay of the mean axial velocity profile for the q vortex for case B, where the initial perturbation consists of high-amplitude random disturbances.

opments of the axial and tangential velocities for case A. In the core, the mean axial velocity deficit is weakened, while the mean tangential velocity is strengthened. This pushes the vortex toward a stable configuration, and shows the relative insignificant impact of an unstable stability wave on the tangential velocity field of the vortex. The velocity profiles for case B are shown in Figs. 12 and 13. While there is a reduction in the axial velocity deficit, there is no significant change in the tangential profile. In order to ascertain that it is indeed the growth of the disturbance and its interaction with the mean flow that caused the decay of axial velocity deficit, we simulated an unstable q vortex ($q=1$) with no initial perturbations. The evolution of the mean axial centerline velocity is shown in Fig. 14 for cases A and B, along with the case with no initial perturbations. It is evident that while

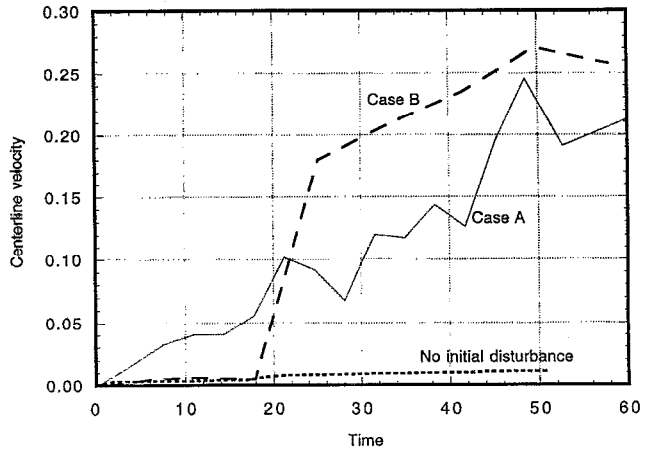

FIG. 14. Evolution of the mean centerline axial velocity for different initial conditions.

cases A and B developed a strong increase of the axial velocity at the center, the vortex with no initial disturbances showed a negligible change. It should be noted here that an increase in the axial velocity at the center amounts to a corresponding decrease in the axial velocity deficit. Therefore, the growth of the large-scale structures causes the redistribution of both the angular and axial momentum between the core and surroundings. The redistribution results in a more stable vortex than the initial mean flow.

In Fig. 15, the normalized circulation profile for case A at $T=75$ is compared with the "universal inner region" described by Hoffman and Joubert.[26] The power region and the logarithmic region are both visible. To better see the logarithmic region, the parameter $C=(\Gamma/\Gamma_1-1)/\ln(r/r_1)$ is plotted as function of r/r_1 in Fig. 16. Here Γ_1 and r_1 are the circulation and radius at the location of maximum tangential velocity. This parameter should be exactly one in the loga-

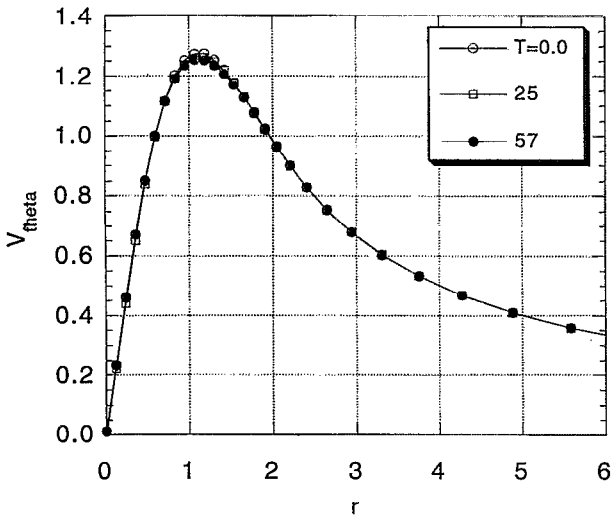

FIG. 13. Evolution of the mean tangential velocity profile for the q vortex for case B, where the initial perturbation consists of high-amplitude random disturbances.

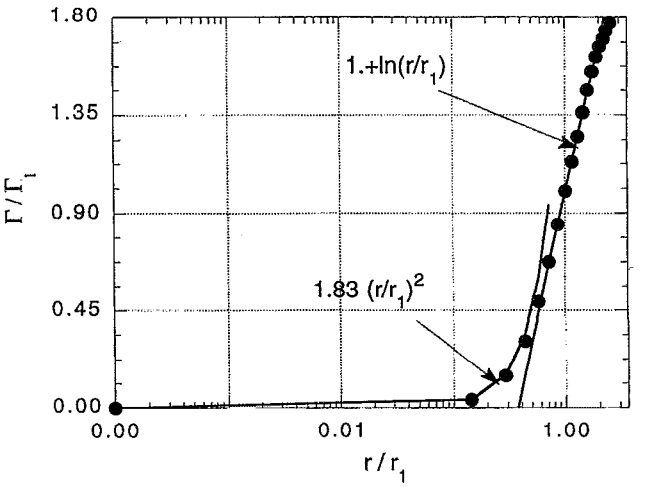

FIG. 15. Comparison of normalized mean circulation profile with the experimental profile of Hoffman and Joubert for the q vortex. The inner power region and the logarithmic region are visible. The circles denote the present numerical simulation. $Time=75$. The mean flow is perturbed with the (1,1) mode.

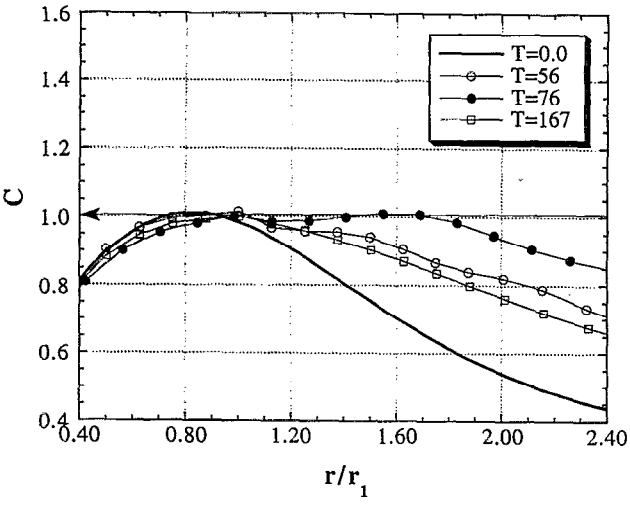

FIG. 16. Comparison of C in the empirical formula of Hoffman and Joubert for the q vortex. Here $C=(\Gamma/\Gamma_1-1)/\ln(r/r_1)$ should be exactly one in the logarithmic region. Note that the initial profile has no logarithmic region. The mean flow is perturbed with the (1,1) mode.

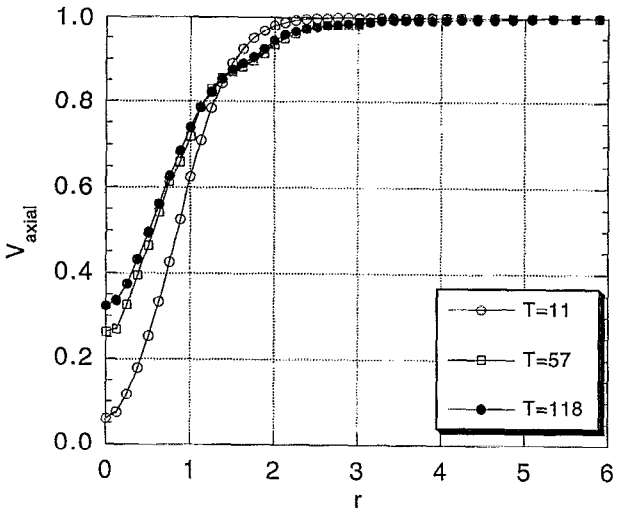

FIG. 18. Decay of the mean axial velocity profile for the q vortex, where the initial perturbation consists of the (1,1) mode, DNS.

rithmic region. At $T=0$, there is no logarithmic region. Later in time, when the turbulent kinetic energy is a maximum, a logarithmic region is seen extending from $r/r_1=0.8$ to $r/r_1=1.4$. Saffman,[27] in his theoretical analysis, places the logarithmic region between 0.8 and 1.2. As the turbulent kinetic energy decays, the logarithmic region disappears, indicating relaminarization of the vortex. For case B, since the vortex did not generate any significant turbulence levels, the formation of a logarithmic region was not evident.

E. Direct numerical simulation

A direct numerical simulation was performed at a lower Reynolds number to substantiate the conclusions reached using LES. The computational domain and the reference parameters are the same as case A. However, the Reynolds number based on the core parameters is 4000. A grid of $(73\times129\times129)$ is used. As mentioned earlier, spectral and sixth-order compact differencing are used in the periodic streamwise direction and the other two directions in the cross-plane, respectively. A third-order low-storage Runge–Kutta scheme is used for the time integration. The computed energy spectra and instantaneous velocity profiles show that the turbulence is well resolved by this grid.

The evolution of the large-scale structures and the turbulent kinetic energy showed similar development as case A. Figure 17 shows the distribution of turbulent kinetic energy E at different times. It also shows the same trend as Fig. 6, which shows the evolution of the same quantity for case A. But the maximum kinetic energy attained at the center is lower than that of case A. This is expected because of the

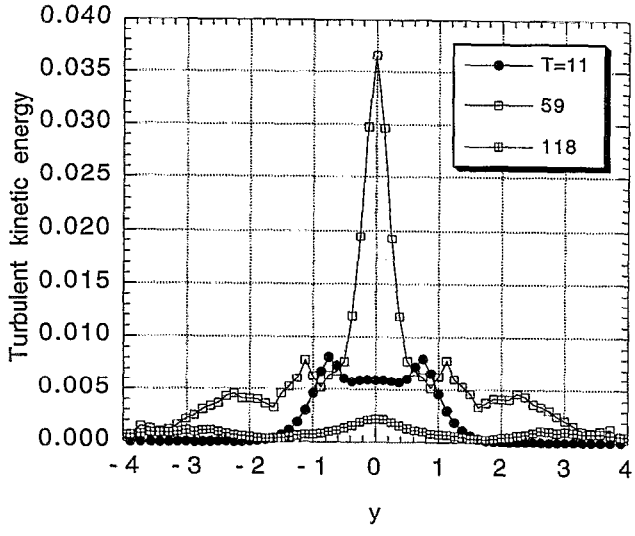

FIG. 17. Radial distribution of turbulent kinetic energy for the q vortex at different times. The flow is perturbed with the (1,1) mode, DNS.

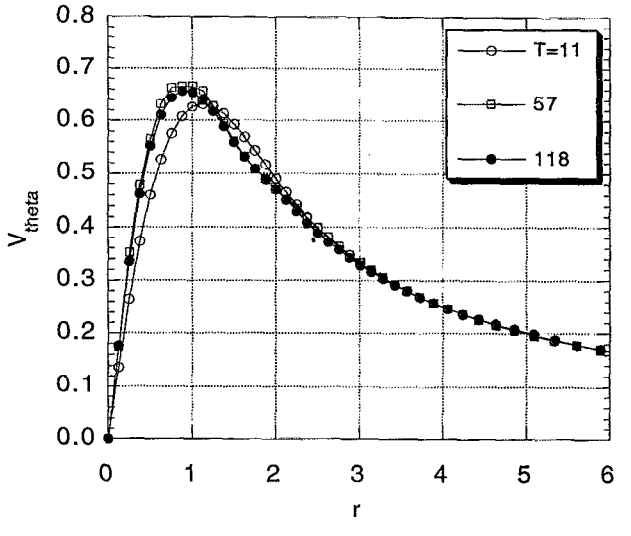

FIG. 19. Evolution of the mean tangential velocity profile for the q vortex, where the initial perturbation consists of (1,1) mode, DNS.

lower Reynolds number used in the DNS. The mean flow profiles also show a similar trend. Figure 18 shows the decrease in the axial velocity deficit with time, which is consistent with the LES results. The evolution of the mean tangential velocity profiles shown in Fig. 19 also confirms the LES results. The redistribution of the axial and the angular momentum between the core region and surrounding is evident, and is consistent with the LES results.

IV. CONCLUSIONS

The q vortex is used as a model for a trailing vortex with an axial velocity deficit. The tangential velocity field of the q vortex has a monotone radial variation of circulation, which makes the vortex centrifugally neutrally stable. The instability mechanism in this vortex is due to the presence of the axial velocity deficit. Results have been obtained for $q=1$ using temporal LES. It is found that a linearly unstable q vortex amplifies the perturbations, resulting in the formation of large-scale structures. These structures appear as helical sheets of vorticity sprouting out of the vortex core. Later, these structures break up into small-scale motions in the form of helical filaments. The small-scale motions are predominant near the core radius. In the core, the axial velocity deficit is weakened and the swirling flow is strengthened due to the redistribution of axial and angular momentum between the core and the surroundings. Subsequently, the stabilizing motion of the core "wins" over the destabilizing effects of the axial velocity. The vortex returns eventually to a laminar state, but with a weakened axial-velocity deficit.

The turbulent kinetic energy shows a strong growth during the initial stages, due to amplification of the instability waves, but later it saturates and a period of slow decay prevails. Initially only the instability wave that is seeded shows strong growth. But later, other waves start to appear due to nonlinear interactions. Subsequently, the modal kinetic energies of all the modes saturate. A period of slow decay then prevails.

During the period of amplification and decay of disturbances, the mean tangential velocity profile shows no significant decay. However, the axial velocity profile shows a decrease in the deficit, indicating the weakening of the instability mechanism. During the period of maximum turbulent kinetic energy, the normalized circulation profile shows the formation of a logarithmic region and compares well with the "universal inner region" of Hoffman and Joubert.[26]

When a linearly stable q vortex ($q=2$) is perturbed with high-amplitude random disturbances, no significant structures are generated. The mean tangential velocity profile shows no decay, while the mean axial velocity shows a decrease in the velocity deficit.

A temporal direct numerical simulation of an unstable q vortex ($q=1$) performed at a lower Reynolds number confirms the trends observed in the LES results.

ACKNOWLEDGMENT

This work is supported by the Office of Naval Research under Grant No. N00014-92-J-4087.

[1]Lord Rayleigh, "On the dynamics of revolving fluids," Proc. R. Soc. London Ser. A **93**, 148 (1916).
[2]R. Panton, *Incompressible Flow* (Wiley, New York, 1984).
[3]M. K. Sreedhar and S. A. Ragab, "Large-eddy simulation of a stationary longitudinal vortex," Phys. Fluids **6**, 2501 (1994).
[4]G. K. Batchelor and A. E. Gill, "Analysis of the stability of axisymmetric jets," J. Fluid Mech. **14**, 529 (1962).
[5]M. S. Uberoi, C. C. Chow, and J. P. Narain, "Stability of coaxial rotating jet and vortex of different densities," Phys. Fluids **15**, 1718 (1972).
[6]J. P. Narain and M. S. Uberoi, "Nonlinear stability of cylindrical vortex enclosing a central jet of light or dense fluid," Phys. Fluids **16**, 1406 (1973).
[7]P. I. Singh and M. S. Uberoi, "Experiments on vortex stability," Phys. Fluids **19**, 1858 (1976).
[8]G. K. Batchelor, "Axial flow in trailing line vortices," J. Fluid Mech. **20**, 321 (1964).
[9]M. R. Lessen, P. J. Singh, and F. Paillet, "The stability of a trailing line vortex. Inviscid theory," J. Fluid Mech. **63**, 753 (1974).
[10]M. R. Lessen and F. Paillet, "The stability of a trailing line vortex. Viscous theory," J. Fluid Mech. **65**, 769 (1974).
[11]P. W. Duck and M. R. Foster, "The inviscid stability of a trailing line vortex," J. Appl. Math. Phys. **31**, 524 (1980).
[12]M. R. Khorrami, "On the viscous modes of instability of a trailing vortex," J. Fluid Mech. **225**, 197 (1991).
[13]P. W. Duck and M. R. Khorrami, "On the effects of viscosity on the stability of a trailing line vortex," ICASE Report No. 91-6, NASA Langley Research Center, 1991.
[14]E. W. Mayer and K. G. Powell, "Viscous and inviscid instabilities of a trailing vortex," J. Fluid Mech. **245**, 91 (1992).
[15]K. Stewartson, "The stability of swirling flows at large Reynolds number when subjected to disturbances with large azimuthal wavenumber," Phys. Fluids **25**, 1953 (1982).
[16]S. Leibovitch and K. Stewartson, "A sufficient condition for the instability of columnar vortices," J. Fluid Mech. **126**, 335 (1983).
[17]J. Smagorinsky, "General circulation experiments with the primitive equations. I. The basic experiment," Mon. Weather Rev. **91**, 99 (1963).
[18]M. Germano, U. Piomelli, P. Moin, and W. Cabot, "A dynamic subgrid-scale eddy viscosity model," Phys. Fluids A **3**, 1760 (1991).
[19]G. Erlebacher, M. Y. Hussaini, C. G. Speziale, and T. A. Zang, "Toward the large-eddy simulation of compressible turbulent flows," J. Fluid. Mech. **238**, 155 (1992).
[20]M. K. Sreedhar, "Large-eddy simulation of a turbulent vortices and free shear layers," Ph.D. dissertation, Virginia Polytechnic Institute and State University, Blacksburg, Virginia, 1994.
[21]D. Gottlieb and E. Turkel, "Dissipative two–four methods for time-dependent problems," Math. Comput. **30**, 703 (1976).
[22]S. A. Ragab, S. Sheen, and M. Sreedhar, "An investigation of finite-difference methods for large-eddy simulation of a mixing layer," AIAA Paper No. 92-0554, 1992.
[23]S. K. Lele, "Compact finite difference schemes with spectral like resolution," Center for Turbulence Research Manuscript-107, Stanford University, Stanford, CA, April 1990.
[24]P. Bandyopadhyay, D. Stead, and R. Ash, "The organized nature of turbulent trailing vortex," AIAA Paper No. 90-1625, 1990.
[25]W. J. Devenport, M. C. Rife, S. I. Liapis, and J. Miranda, "Turbulent trailing vortex," AIAA Paper No. 94-0404, 1994.
[26]E. R. Hoffman and P. N. Joubert, "Turbulent line vortices," J. Fluid Mech. **16**, 395 (1963).
[27]P. G. Saffman, "Structure of turbulent line vortices," Phys. Fluids **16**, 1181 (1973).